Characterization of Magnetic Plasmons in Extended Metal Nanoparticle Oligomers

Nicholas P. Montoni,[†] Steven C. Quillin,[†] Charles Cherqui,[†] and David J. Masiello[*,†,‡]

Department of Chemistry, University of Washington, Seattle, WA 98195, and Department of Applied Mathematics, University of Washington, Seattle, WA 98195

E-mail: masiello@chem.washington.edu

Abstract

Ring-like assemblies of metal nanoparticles that exhibit magnetic resonances, called magentic plasmon oligomers, have been of recent interest as negative-index metamaterials. Magnetic plasmon oligomers have potential applications in cloaking, superlensing, information transmission, and sensing. For these reasons, it is imperative to understand the properties of such systems on both small and large scales. We show through theory and simulation that the energy ordering of the magnetic resonances of small oligomers depends greatly on the size and scale of the nanoparticle assembly in ways that purely electric plasmons do not. We verfiy that this is the result of retardation effects, and assert that any qualitatively accurate description of magnetic plasmons must incorporate retardation effects. We culminate this study with a parametrization of the fully retarded, magnetic-magnetic dipole coupling between oligomers, providing a route to characterizing extended chains and arrays of magnetic plasmon oligomers.

[*]To whom correspondence should be addressed
[†]Department of Chemistry, University of Washington
[‡]Department of Applied Mathematics, University of Washington

Bringing two or more metal nanoparticles (MNPs) together allows their individual electric plasmons to hybridize, producing a new set of plasmonic modes.[2–5] Plasmon hybridization theory is applied to aggregates of MNPs and explains their collective behavior within the quasistatic limit in which the speed of light is taken to be infinite.[6–9] Recently, retardation effects on plasmon hybridization have been the focus of study for large particles[11,14] as well as dimers,[10,12,15] and 2-D arrays[13,16,17] of nanoparticles. Specific arrangements of nanoparticles in 2-D arrays, such as three or more nanoparticles arranged on the vertices of a regular polygon, support a collective mode in which all of the dipole plasmons are oriented head-to-tail. This generates a fictitious, oscillating current loop resulting in an oscillating magnetic dipole moment in the center of the ring.[18–22] These so-called magnetic plasmons are the lowest-energy collective modes of the oligomers and couple to and enhance the magnetic field of incident light,[23–25] offering a route to applications such as solar cell enhancement,[26–28] biosensing and detection,[29–36] and information storage and propagation.[37–39] The rich plasmonic modes of magnetic-plasmon-supporting systems are well-described using plasmon hybridization theory, but when in the quasistatic limit, the energy-ordering of the modes is not.

Plasmon hybridization theory treats LSPRs as point dipoles centered on their associated nanoparticles that interact through dipole-dipole coupling. In the quasistatic limit, these dipoles couple only through time-independent, electric near-field interactions,[41] but when the size of and distance between nanoparticles becomes large, this approximation breaks down and intermediate- and far-field effects must be considered, as well as the time-delay effects in the near-field.[41] The aim of this paper is to incorporate the fully retarded electric field into plasmon hybridization theory and extend studies of retardation effects to magnetic plasmon oligomers. Specifically, we explore oligomers comprising two and three rings of nanoparticles and compare to full-wave simulation[?] to verify that our approach qualitatively predicts the energy-ordering of the magnetic modes.[22]

For all following magnetic oligomers, only the two planar dipoles per particle are consid-

ered in the tight binding model. The dipoles are mapped onto a set of harmonic oscillators and are described by the following Hamiltonian:

$$H = \sum_{i}^{n} \frac{\mathbf{P}_i^2}{2m_{\mathrm{sp,i}}} + \frac{1}{2} m_{\mathrm{sp,i}} w_{textrmsp,i}^2 \mathbf{X}_i^2 + e^2 \sum i \neq j \mathbf{X}_i \cdot \mathbf{\Lambda}_{\mathrm{full},ij} \cdot \mathbf{X}_j \tag{1}$$

where $\mathbf{P}_i$ are the momenta conjugate to the coordinates $\mathbf{X}_i$, $\omega_{sp,i}$ are the individual LSPR frequencies of each oscillator, $m_{sp,i}$ are the LSPR effective masses and $\mathbf{\Lambda}_{\mathrm{full},ij}$ is the fully retarded dipole dipole realy tensor. To make this Hamiltonian more manageable, it is nondimensionalized using $\mathbf{Q}_i = (m_{\mathrm{sp}}\omega_{\mathrm{sp}}/\hbar)^{\frac{1}{2}}\, \mathbf{X}_i$ and $\mathbf{\Pi}_i = \mathbf{P}_i/\sqrt{\hbar m_{\mathrm{sp}}\omega_{\mathrm{sp}}}$. Substituting into [EQUATION REF] and expanding $\mathbf{\Lambda}_{\mathrm{full},ij}$, we get:

$$H = \frac{\hbar\omega_{sp}}{2} \sum_{i}^{n} [\mathbf{\Pi}_i^2 + \mathbf{Q}_i^2] - \frac{\hbar\omega_{sp}}{2} \sum_{i \neq j} \{ g_{ij}^{NF} \left[3(\mathbf{Q}_i \cdot \hat{\mathbf{n}}_{ij})(\hat{\mathbf{n}}_{ij} \cdot \mathbf{Q}_j) - \mathbf{Q}_i \cdot \mathbf{Q}_j \right] + g_{ij}^{IF} \left[3(\mathbf{Q}_i \cdot \hat{\mathbf{n}}_{ij})(\hat{\mathbf{n}}_{ij} \cdot \mathbf{Q}_j) - \mathbf{Q}_i \cdot \mathbf{Q}_j \right. \tag{2}$$

In this Hamiltonian we introduce the near, intermediate, and far-field coupling terms: $g_{ij}^{NF} = \frac{\alpha_{sp}}{r_{ij}^3} \cos\left(\frac{\omega r_{ij}}{c}\right)$, $g_{ij}^{IF} = \frac{\alpha_{sp}\omega}{r_{ij}^2 c} \sin\frac{\omega r_{ij}}{c}\big)$, and $g_{ij}^{FF} = \frac{\alpha_{sp}\omega^2}{r_{ij}c^2} \cos\frac{\omega r_{ij}}{c}\big)$, respectively. Additionally, the polarizability $\alpha_{sp} = \frac{e^2}{m_{sp}\omega_{sp}^2}$, r_{ij} is the distance between the ith and jth LSPs, and $\hat{\mathbf{n}}_{ij}$ is the unit vector connecting two LSPs. The first systems we examine are the magnetic dimer introduced in Cherqui's 2014 work, a three-ring chain, and three rings arranged in a triangle. Because we are interested in the effects of scale, we must define a scaling parameter for the system. The ten MNPs arranged at the vertices of two fused hexagons [PUT A FIGURE HERE, PROBABLY] each have radius a_0 and are separated by lattice spacing $r = 2.2 \times a_0$. With the radius of the particles defining the scale of the system, there now exists a way to probe the energy ordering of the modes as a function of size.

In the theoretical studies of Cherqui *et al.*,[22] it was found using the quasistatic tight-binding model described above that the magnetic dimer system supports twenty planar modes, with the two lowest-energy modes, denoted north-south (NS) and north-north (NN), exhibiting magnetic character. The NS mode supports two out-of-phase effective current

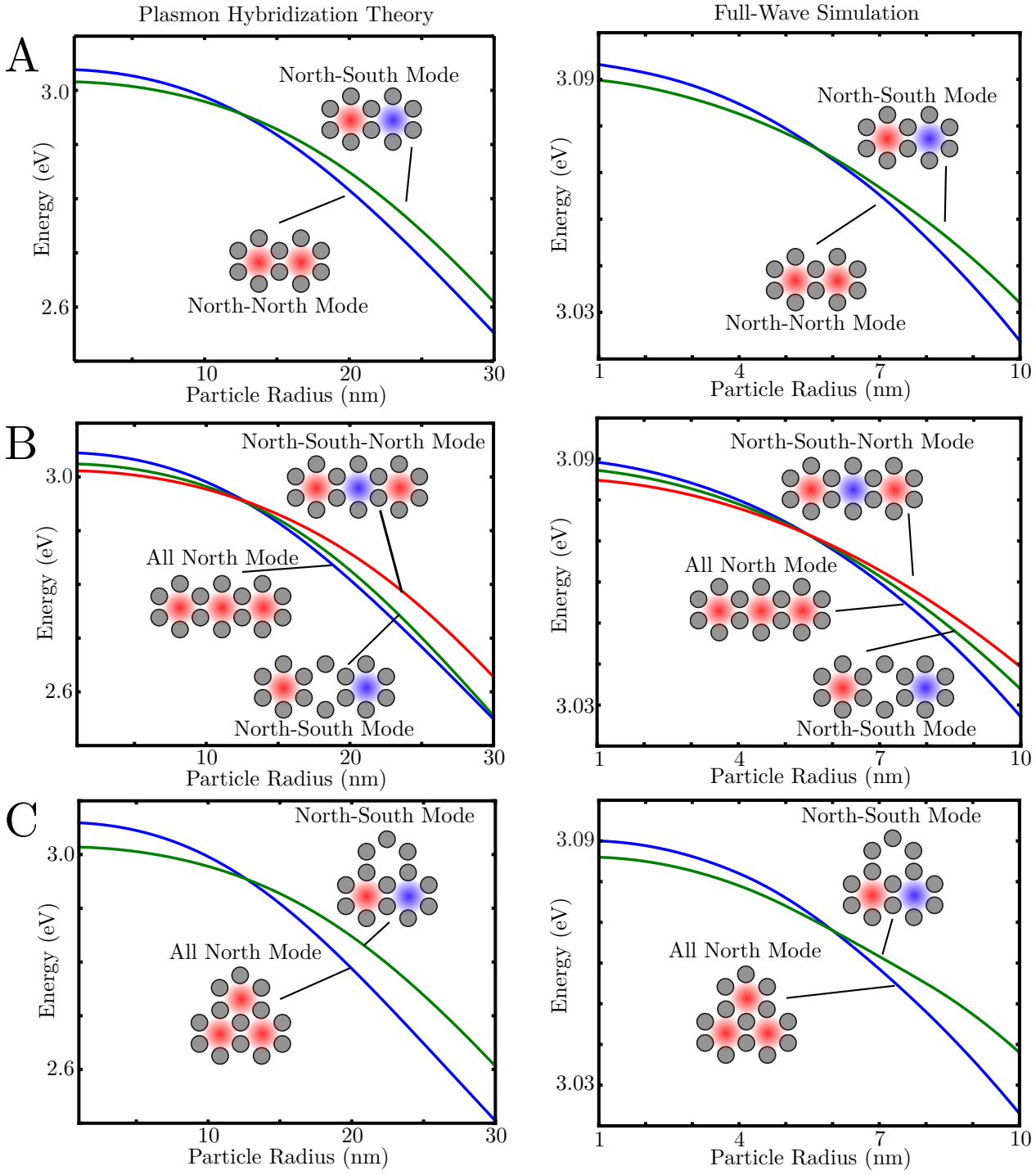
Plasmon Hybridization Theory
Full-Wave Simulation
A
B
C
North-South Mode
North-North Mode
North-South-North Mode
All North Mode
Energy (eV)
Particle Radius (nm)
3.0
2.6
3.09
3.03
10
20
30
1
4
7
10

loops and, consequently, out-of-phase magnetic moments in each ring. The NN mode supports a single, in-phase, effective current loop about the entire system, generating two in-phase magnetic dipole moments within the rings.

However, at odds with the tight-binding model results, previous full-wave electrodynamics simulations conclude the opposite: the NN mode lies at lower energy than the NS mode. This discrepancy is the result of retardation effects, as the original tight-binding model uses the quasistatic approximation, while the simulations use the fully retarded electric field. Because retardation effects contribute more with growing size, small systems behave predictably within the quasistatic approximation and the NS mode is the lowest in energy. At larger sizes, when retardation effects contribute, the NN mode is the lowest in energy. In the quasistatic limit, the tight-binding model accurately predicts the eigenmodes of the dimer, but is unable to account for the variation in each mode's eigenvalue as a function of size.

The electric field in the quasistatic approximation is proportional to $\frac{1}{r^3}$, dictating that nearest-neighbor interactions dominate the dipole-dipole coupling. In both the NN and NS mode, all of the nearest-neighbor interactions are "bonding," or energetically preferred. These two modes differ at the central two particles where the NS mode exhibits head-to-tail, collinear dipoles, while in the NN mode supports anti-parallel dipoles. The $3(\mathbf{p}_2 \cdot \hat{\mathbf{r}})(\hat{\mathbf{r}} \cdot \mathbf{p}_1)$ term in the coupling dictates that collinear dipoles are more energetically preferable than anti-parallel dipoles. As a result, the NS mode is energetically preferred, followed by the NN mode. When the fully retarded field is taken into account, all inter-particle interactions contribute to the energy-ordering.

The fully retarded electric field is composed of three parts: the near-field term (Equation 2), the intermediate-field term (Equation 3), and the far-field term (Equation 4). The intermediate-field term contributes the same energy ordering as the near-field term: collinear dipoles are favored more than anti-parallel dipoles. The far-field term, however, is energetically unfavorable for anti-parallel interactions and energetically preferable for parallel

interactions. These three terms account for all of the retardation effects.[42]

To understand the contributions to dipole-dipole coupling of each part of the fully retarded electric field, the interaction strengths for each term were computed for four planar hybridized modes of a silver nanosphere dimer. The results of these computations are displayed in and show how the interaction terms behave in various size regimes. The most obvious trait to note is that the far-field term is zero for both collinear and anti-collinear arrangements of dipoles. Second, the collinear and anti-collinear interactions are exact opposites of each other, with the same being true for the parallel and anti-parallel arrangements, as these represent equal and opposite interactions. Third the interaction strengths have slow oscillatory behavior over long length scales. Fourth, and perhaps most importantly, there are distinct distance regimes in which each term is more energetically favorable than the others. This final observation lends credence to the idea that the long-distance interactions in the NN mode are more favorable than those in the NS mode.

Incorporating the fully retarded electric field, the inter-particle coupling is no longer approximately a nearest-neighbor interaction, but rather a short- and long-distance coupling that accounts for the interactions among all particles. As the system grows larger, intermediate- and far-field interactions become stronger in proportion to the dominant near-field interactions.

Returning to the tight-binding model, retardation effects are included by using the full interaction term in the Hamiltonian. The interaction terms depend on ω, the frequency at which the collective mode resonates. This means that the Hamiltonian must now be diagonalized iteratively, beginning by using the LSPR frequency ω_{sp} of a sphere and resubstituting the resonant frequency of the mode of interest until the value converges. Additionally, the contribution of radiation damping[15] is introduced by adding a term to the bulk damping coefficient proportional to $\tau = \frac{2e^2}{3m_{sp}c^3}$ which causes a slight redshift in the LSPR frequency. Figure 4 tracks the eigenvalues of the NN and NS mode as a function of radius using the full Hamiltonian. The nanoparticle radius ranges from 1 nm to 20 nm, and the center-to-center

distance between nanoparticles is always $2.2\,r_0$, as in the diagram in Figure 1. Below 10 nm, NS is the lowest-energy mode. Between 10 and 11 nm, the eigenvalues cross, and from 11 nm onward NN is the lowest-energy mode.

This is further verified by full-wave electrodynamics simulations.[43] EELS simulations on magnetic dimer systems of different sizes show that in the quasistatic limit the NN mode is always higher in energy than the NS mode. Conversely, fully retarded simulations show that the NN mode eventually redshifts past the NS mode with increasing dimer size. Because the NS and NN modes are energetically nearly degenerate and their linewidths are broad, a Drude model for silver with a reduced damping coefficient was used as the dielectric function for the spheres. Running simulations for sphere radii between 1 nm and 10 nm and separation distances of $2.2\,r_0$, it is found that the NN mode redshifts past the NS mode between 5 and 10 nm. The simulated EEL spectra are presented in Figure **??**. In the quasistatic limit, just as predicted, the modes did not change in energy with increasing particle size, due to the fact that the separation distances are parameterized by the radius. The interaction energy scales as $\frac{1}{r_0^3}$ and the polarizability scales as r_0^3, so these effects directly cancel and the modes do not change with increasing particle size in the quasistatic limit.

It has been shown that for small magnetic oligomer systems, specifically naphthalene-like decamers of silver nanospheres, quasistatic plasmon hybridization theory and fully retarded, full-wave numerical simulations agree on the energy-ordering of the magnetic modes. However, as the individual nanoparticles become larger and proportionally farther apart, the quasistatic limit breaks down and the simulations predict a different energy-ordering than the tight-binding model. Introducing retardation effects into the tight-binding model requires including the time-dependence of the near-field as well as the entire intermediate- and far-field terms. Consideration of these retardation effects also introduces radiation damping, which further impacts the resonant frequencies and broadening of the collective modes. Implementing this and iteratively solving for the eigenvalues of the collective magnetic modes, it is shown that including the fully retarded electric field properly predicts the energy-ordering

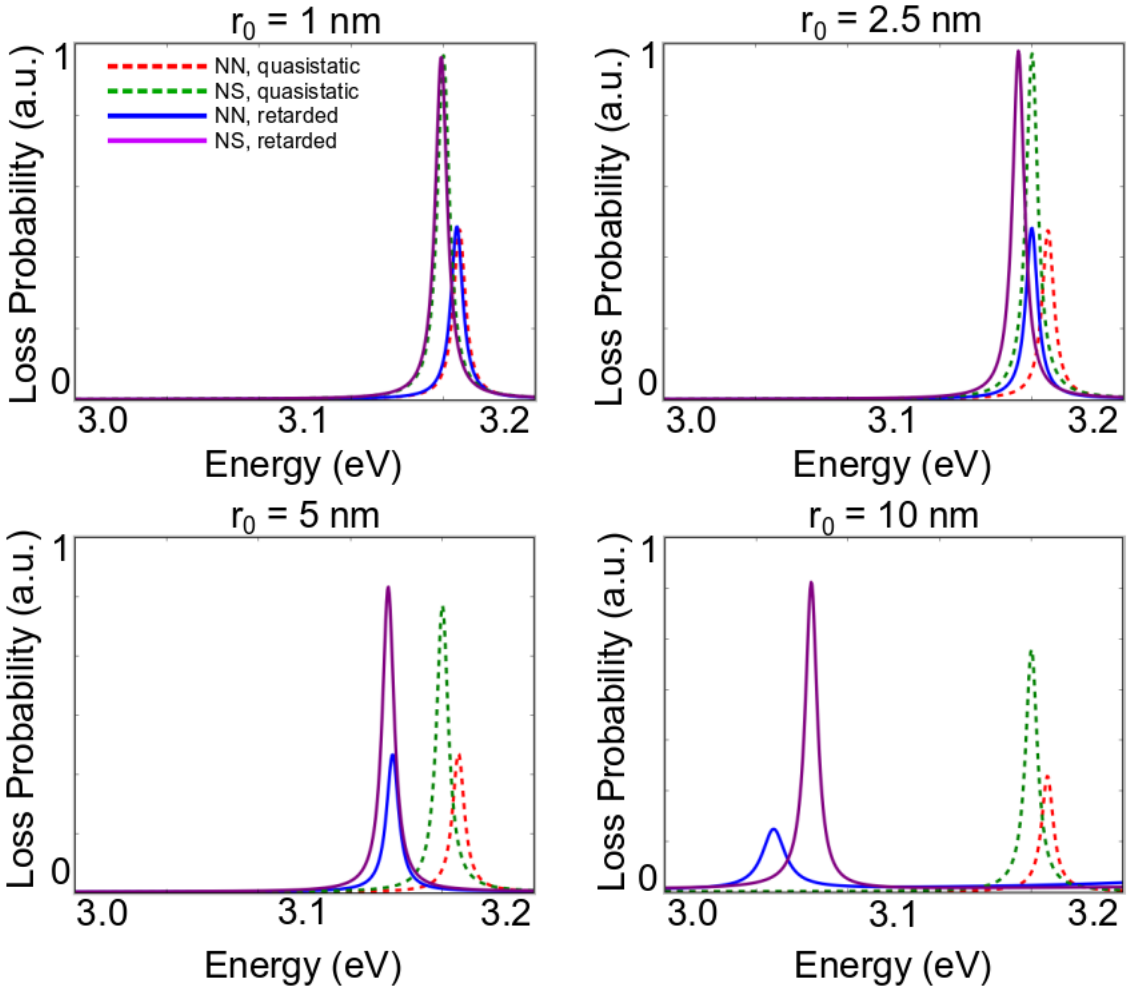

Figure 1: Simulated quasistatic and fully retarded EEL spectra for the magnetic dimer with $r_0 = 1$ nm, 2.5 nm, 5 nm, and 10 nm. When the particles are very small, the quasistatic NS (green) and NN (red) modes are nearly energetically degenerate with the fully retarded NS (purple) and NN (blue) modes. As the size increases, the red and green traces do not move, but the purple and blue traces begin to redshift. Between 5 and 10 nm, the blue trace redshifts past the purple trace, indicating that in this size regime the NN mode is energetically favorable.

in agreement with simulation. This gives a new route to the qualitative characterization of large, multi-constituent nanoparticle aggregates and accurately predicting the energy-ordering of the collective modes in various size regimes.

Acknowledgement

Thanks mom and dad, also whoever paid us. Thanks Masiello group for being cool. Thanks for not barfing after you read this. And thanks Hillary Clinton for being my idol.

References

(1) Kreibig, U.; Genzel, L. Optical absorption of small metallic particles. *Surface Science* **1985**, *156*, 678 – 700.

(2) Clippe, P.; Evrard, R.; Lucas, A. A. Aggregation effect on the infrared absorption spectrum of small ionic crystals. *Phys. Rev. B* **1976**, *14*, 1715–1721.

(3) Aravind, P.; Nitzan, A.; Metiu, H. The interaction between electromagnetic resonances and its role in spectroscopic studies of molecules adsorbed on colloidal particles or metal spheres. *Surface Science* **1981**, *110*, 189 – 204.

(4) Xu, Y. Electromagnetic scattering by an aggregate of spheres. *Appl. Opt.* **1995**, *34*, 4573–4588.

(5) Mishchenko, M. I.; Mackowski, D. W.; Travis, L. D. Scattering of light by bispheres with touching and separated components. *Appl. Opt.* **1995**, *34*, 4589–4599.

(6) Prodan, E.; Radloff, C.; Halas, N. J.; Nordlander, P. A Hybridization Model for the Plasmon Response of Complex Nanostructures. *Science* **2003**, *302*, 419–422.

(7) Prodan, E.; Nordlander, P. Plasmon hybridization in spherical nanoparticles. *The Journal of Chemical Physics* **2004**, *120*, 5444–5454.

(8) Nordlander, P.; Oubre, C.; Prodan, E.; Li, K.; Stockman, M. I. Plasmon Hybridization in Nanoparticle Dimers. *Nano Letters* **2004**, *4*, 899–903.

(9) Davis, T. J.; Vernon, K. C.; Gómez, D. E. Designing plasmonic systems using optical coupling between nanoparticles. *Phys. Rev. B* **2009**, *79*, 155423.

(10) Kottmann, J. P.; Martin, O. J. F. Retardation-induced plasmon resonances in coupled nanoparticles. *Opt. Lett.* **2001**, 1096–1098.

(11) Turner, M. D.; Hossain, M. M.; Gu, M. The effects of retardation on plasmon hybridization within metallic nanostructures. *New Journal of Physics* **2010**, *12*, 083062.

(12) Rechberger, W.; Hohenau, A.; Leitner, A.; Krenn, J.; Lamprecht, B.; Aussenegg, F. Optical properties of two interacting gold nanoparticles. *Optics Communications* **2003**, *220*, 137 – 141.

(13) Kinnan, M. K.; Chumanov, G. Plasmon Coupling in Two-Dimensional Arrays of Silver Nanoparticles: II. Effect of the Particle Size and Interparticle Distance. *The Journal of Physical Chemistry C* **2010**, *114*, 7496–7501.

(14) Myroshnychenko, V.; Rodriguez-Fernandez, J.; Pastoriza-Santos, I.; Funston, A. M.; Novo, C.; Mulvaney, P.; Liz-Marzan, L. M.; Garcia de Abajo, F. J. Modelling the optical response of gold nanoparticles. *Chem. Soc. Rev.* **2008**, *37*, 1792–1805.

(15) Dahmen, C.; Schmidt, B.; von Plessen, G. Radiation Damping in Metal Nanoparticle Pairs. *Nano Letters* **2007**, *7*, 318–322, PMID: 17243751.

(16) Haynes, C. L.; McFarland, A. D.; Zhao, L.; Van Duyne, R. P.; Schatz, G. C.; Gunnarsson, L.; Prikulis, J.; Kasemo, B.; Käll, M. Nanoparticle Optics: The Importance of Radiative Dipole Coupling in Two-Dimensional Nanoparticle Arrays. *The Journal of Physical Chemistry B* **2003**, *107*, 7337–7342.

(17) Bouhelier, A.; Bachelot, R.; Im, J. S.; Wiederrecht, G. P.; Lerondel, G.; Kostcheev, S.; Royer, P. Electromagnetic Interactions in Plasmonic Nanoparticle Arrays. *The Journal of Physical Chemistry B* **2005**, *109*, 3195–3198, PMID: 16851340.

(18) Alù, A.; Salandrino, A.; Engheta, N. Negative effective permeability and left-handed materials at optical frequencies. *Opt. Express* **2006**, *14*, 1557–1567.

(19) Alù, A.; Engheta, N. Dynamical theory of artificial optical magnetism produced by rings of plasmonic nanoparticles. *Phys. Rev. B* **2008**, *78*, 085112.

(20) Hentschel, M.; Dregely, D.; Vogelgesang, R.; Giessen, H.; Liu, N. Plasmonic Oligomers: The Role of Individual Particles in Collective Behavior. *ACS Nano* **2011**, *5*, 2042–2050, PMID: 21344858.

(21) Brandl, D. W.; Mirin, N. A.; Nordlander, P. Plasmon modes of nanosphere trimers and quadrumers. *The Journal of Physical Chemistry B* **2006**, *110*, 12302–12310.

(22) Cherqui, C.; Bigelow, N. W.; Vaschillo, A.; Goldwyn, H.; Masiello, D. J. Combined tight-binding and numerical electrodynamics understanding of the STEM/EELS magneto-optical responses of aromatic plasmon-supporting metal oligomers. *ACS Photonics* **2014**, *1*, 1013–1024.

(23) Shalaev, V. M. Optical negative-index metamaterials. *Nature photonics* **2007**, *1*, 41–48.

(24) Qian, Z.; Hastings, S. P.; Li, C.; Edward, B.; McGinn, C. K.; Engheta, N.; Fakhraai, Z.; Park, S.-J. Raspberry-like metamolecules exhibiting strong magnetic resonances. *ACS nano* **2015**, *9*, 1263–1270.

(25) Urzhumov, Y. A.; Shvets, G.; Fan, J. A.; Capasso, F.; Brandl, D.; Nordlander, P. Plasmonic nanoclusters: a path towards negative-index metafluids. *Optics express* **2007**, *15*, 14129–14145.

(26) Graydon, O. Solar cells: Fano-enhanced performance. *Nature Photonics* **2011**, *6*, 4.

(27) Le, K. Q.; Alu, A. Fano-induced solar absorption enhancement in thin organic photovoltaic cells. *Applied Physics Letters* **2014**, *105*, 141118.

(28) Le, K. Q.; Bai, J. Enhanced absorption efficiency of ultrathin metamaterial solar absorbers by plasmonic Fano resonance. *JOSA B* **2015**, *32*, 595–600.

(29) Karaveli, S.; Zia, R. Strong enhancement of magnetic dipole emission in a multilevel electronic system. *Optics letters* **2010**, *35*, 3318–3320.

(30) Noginova, N.; Zhu, G.; Mavy, M.; Noginov, M. Magnetic dipole based systems for probing optical magnetism. *Journal of Applied Physics* **2008**, *103*, 07E901.

(31) Wang, J.; Fan, C.; He, J.; Ding, P.; Liang, E.; Xue, Q. Double Fano resonances due to interplay of electric and magnetic plasmon modes in planar plasmonic structure with high sensing sensitivity. *Opt. Express* **2013**, *21*, 2236–2244.

(32) Zhu, Z.; Bai, B.; You, O.; Li, Q.; Fan, S. Fano resonance boosted cascaded optical field enhancement in a plasmonic nanoparticle-in-cavity nanoantenna array and its SERS application. *Light: Science and Applications* **2015**, *4*, e296.

(33) Lee, K.-L.; Huang, J.-B.; Chang, J.-W.; Wu, S.-H.; Wei, P.-K. Ultrasensitive Biosensors Using Enhanced Fano Resonances in Capped Gold Nanoslit Arrays. *Scientific Reports* **2015**, *5*, 8547.

(34) Wu, C.; Khanikaev, A. B.; Adato, R.; Arju, N.; Yanik, A. A.; Altug, H.; Shvets, G. Fano-resonant asymmetric metamaterials for ultrasensitive spectroscopy and identification of molecular monolayers. *Nature Materials* **2012**, *11*, 69–75.

(35) Cetin, A. E.; Altug, H. Fano resonant ring/disk plasmonic nanocavities on conducting substrates for advanced biosensing. *ACS nano* **2012**, *6*, 9989–9995.

(36) Zhang, S.; Bao, K.; Halas, N. J.; Xu, H.; Nordlander, P. Substrate-induced Fano resonances of a plasmonic nanocube: a route to increased-sensitivity localized surface plasmon resonance sensors revealed. *Nano letters* **2011**, *11*, 1657–1663.

(37) Liu, H.; Genov, D. A.; Wu, D. M.; Liu, Y. M.; Steele, J. M.; Sun, C.; Zhu, S. N.; Zhang, X. Magnetic Plasmon Propagation Along a Chain of Connected Subwavelength Resonators at Infrared Frequencies. *Phys. Rev. Lett.* **2006**, *97*, 243902.

(38) Liu, N.; Mukherjee, S.; Bao, K.; Brown, L. V.; Dorfmüller, J.; Nordlander, P.; Halas, N. J. Magnetic plasmon formation and propagation in artificial aromatic molecules. *Nano letters* **2011**, *12*, 364–369.

(39) Liu, N.; Mukherjee, S.; Bao, K.; Li, Y.; Brown, L. V.; Nordlander, P.; Halas, N. J. Manipulating magnetic plasmon propagation in metallic nanocluster networks. *ACS nano* **2012**, *6*, 5482–5488.

(40) Liu, H.; Genov, D. A.; Wu, D. M.; Liu, Y. M.; Liu, Z. W.; Sun, C.; Zhu, S. N.; Zhang, X. Magnetic plasmon hybridization and optical activity at optical frequencies in metallic nanostructures. *Phys. Rev. B* **2007**, *76*, 073101.

(41) Jackson, J. D. *Classical electrodynamics*, 3rd ed.; Wiley: New York, NY, 1999.

(42) Purcell, E. M.; Pennypacker, C. R. Scattering and Absorption of Light by Nonspherical Dielectric Grains. *Astrophys. J.* **1973**, *186*, 705–714.

(43) Hohenester, U.; Trügler, A. MNPBEM - A Matlab toolbox for the simulation of plasmonic nanoparticles. *Computer Physics Communications* **2012**, *183*, 370 – 381.

Graphical TOC Entry

Some journals require a graphical entry for the Table of Contents. This should be laid out "print ready" so that the sizing of the text is correct.
Inside the `tocentry` environment, the font used is Helvetica 8 pt, as required by *Journal of the American Chemical Society*.
The surrounding frame is 9 cm by 3.5 cm, which is the maximum permitted for *Journal of the American Chemical Society* graphical table of content entries. The box will not resize if the content is too big: instead it will overflow the edge of the box.
This box and the associated title will always be printed on a separate page at the end of the document.